TÜBİTAK

**Turkish Journal of Electrical Engineering & Computer Sciences**

http://journals.tubitak.gov.tr/elektrik/

**Research Article**

Turk J Elec Eng & Comp Sci
(2013) 21: 1044 – 1060

doi:10.3906/elk-1106-23

# A real-time extraction of active and reactive current using microcontrollers for a multipulse STATCOM

**Mehmet Ali ANADOL,**[1,*] **Musa AYDIN,**[2] **Tankut YALÇINÖZ**[3]

[1]Technical Science College, Selçuk University, 42003 Konya, Turkey

[2]Department of Electrical and Electronics Engineering, Faculty of Engineering, Selçuk University, 42003 Konya, Turkey

[3]Department of Electrical and Electronics Engineering, Faculty of Engineering, Melikşah University, Talas, 38280 Kayseri, Turkey

**Received:** 09.06.2011 • **Accepted:** 20.03.2012 • **Published Online:** 03.06.2013 • **Printed:** 24.06.2013

**Abstract:** In power transmission and distribution systems, the design of a compensator that adjusts the power factor without causing additional power losses requires the determination of the reactive current components that are going to be supplied into the system. In this study, the determination of the active and reactive current components is achieved via the use of the nonactive power theory and a microcontroller-based control system. The control system has been implemented with low-cost 16-bit microcontrollers. This system was used to control a 3-phase, 12-pulse laboratory-size prototype of a static synchronous compensator (STATCOM) with the structure of a voltage source converter. Verification of the STATCOM and its control circuit were examined via experiments and simulation studies conducted on a single-machine infinite-bus power transmission system. The simulation models for the power and control systems were built by employing the PSCAD/EMTDC program's C programming interface and the graphics-based models in its model library. The experimental results are compared with the results obtained from the PSCAD/EMTDC simulation program.

**Key words:** Flexible AC transmission systems, microcontroller, reactive power compensation, single machine infinite bus, static synchronous compensator

## 1. Introduction

In modern high-voltage power transmission systems, devices called flexible alternating current transmission systems (FACTS) are used for the purposes of smoothing the power quality by adjusting the transmission system parameters (such as impedance, current, or voltage) via advanced converter and control methods, as well as controlling the active and reactive power flow. The static synchronous compensator (STATCOM), which is based on voltage source converters, is one of the most used FACTS devices. The primary objective of the STATCOM is to obtain almost harmonic neutralized and controllable 3-phase AC output voltage wave forms at the point of common coupling (PCC) to regulate the reactive current flow by the generation and absorption of the controllable reactive power by the solid-state switching algorithm [1]. Output voltage waveforms with sufficiently low distortion can be produced by multilevel, multipulse, and pulse-width modulated converters [2]. Depending on the converter structure and compensation requirements, the semiconductor power switches on these converter bridges can be controlled by the implementation of various techniques,

*Correspondence: anadol@selcuk.edu.tr

such as fundamental frequency modulation (FFM), pulse-width modulation (PWM), and selective harmonic elimination (SHE). Both the traditional and modern reference current generation methods developed for the application of these techniques are classified into time- and frequency-domain approaches. A comparison of the performances of these approaches in terms of their advantages and disadvantages, for various cases of current and/or voltage imbalances, was presented in [3,4]. In the literature, the implementation of these methods in the STATCOM control architecture was carried out via microcontroller-based [5] and microcomputer-based [6,7] control cards, which are usually preferred in applications that require complex and advanced computation capabilities. Additionally, the generation of the reference signals and measurement of the electrical quantities can be conducted using 8-bit, 16-bit, or 32-bit microcontrollers. These microcontrollers are preferred in industrial applications, especially because of their low cost, and they are operated compatibly with other peripheral units.

In this study, a microcontroller-based control system is presented for a 3-phase, 12-pulse laboratory-size prototype of a STATCOM with the structure of a voltage source converter (VSC). The nonactive power theory presented in [8] was used to perform real-time reactive power compensation with a multipulse STATCOM. The control system has been implemented with low-cost 16-bit microcontrollers. The validity of the designed control system was verified through experiments and simulation studies conducted on a single-machine infinite bus (SMIB). The results of the experimental studies have been compared with those obtained from the PSCAD/EMTDC simulation programs.

## 2. System overview

Figure 1 shows a general block diagram of the SMIB and a 12-pulse STATCOM being controlled by microcontrollers. As shown in Figure 1, the SMIB system was implemented as 2 overhead transmission lines that have a pi equivalent circuit model with a 360-km length. A dynamic load with P = 308 W, Q = 237 VAR and a STATCOM connected in parallel to this load were placed in the middle of the transmission lines. The STATCOM has been made with 2 units of 3-phase, 6-pulse, voltage-sourced converter bridges. At each leg of the bridge, insulated-gate bipolar transistor (IGBT) power semiconductor switches with reverse parallel diodes are used, which are switched at the AC system frequency (FFM). In addition, in order to prevent overvoltage peaks that may occur on the switches, resistor-capacitor-diode snubber circuits are used in parallel with the converters. These converters are connected at the DC side in parallel with a capacitor. The connection of the 12-pulse converter to the AC grid is made through two 3-phase coupling transformers. The STATCOM's converter bridges were connected to the star and delta secondary windings of these transformers. A 30° phase difference is present between the output voltages of the star- and delta-connected secondary windings of these transformers. The AC output voltages of 6-pulse converters are combined at the primary sides of these transformers for the purpose of eliminating or attenuating the low-level harmonic components. The application of this methodology for the harmonic elimination of a 12-pulse converter is explained in detail in [9].

Reactive power compensation that would enable the drawing of balanced source currents with a unity power factor from the power transmission system can only be obtained with the current control mechanism of the STATCOM [10]. The STATCOM's current control mechanism adjusts the switching angle of the switches on the converter bridges in accordance with the reactive component of the current drawn from the PCC. The reactive current component required for the STATCOM's current control unit was computed using the nonactive power theory and a microcontroller-based control system. A detailed description of the nonactive power theory can be found elsewhere [8,10,11]. The microcontroller-based control system of the STATCOM is described in detail in Section 3.

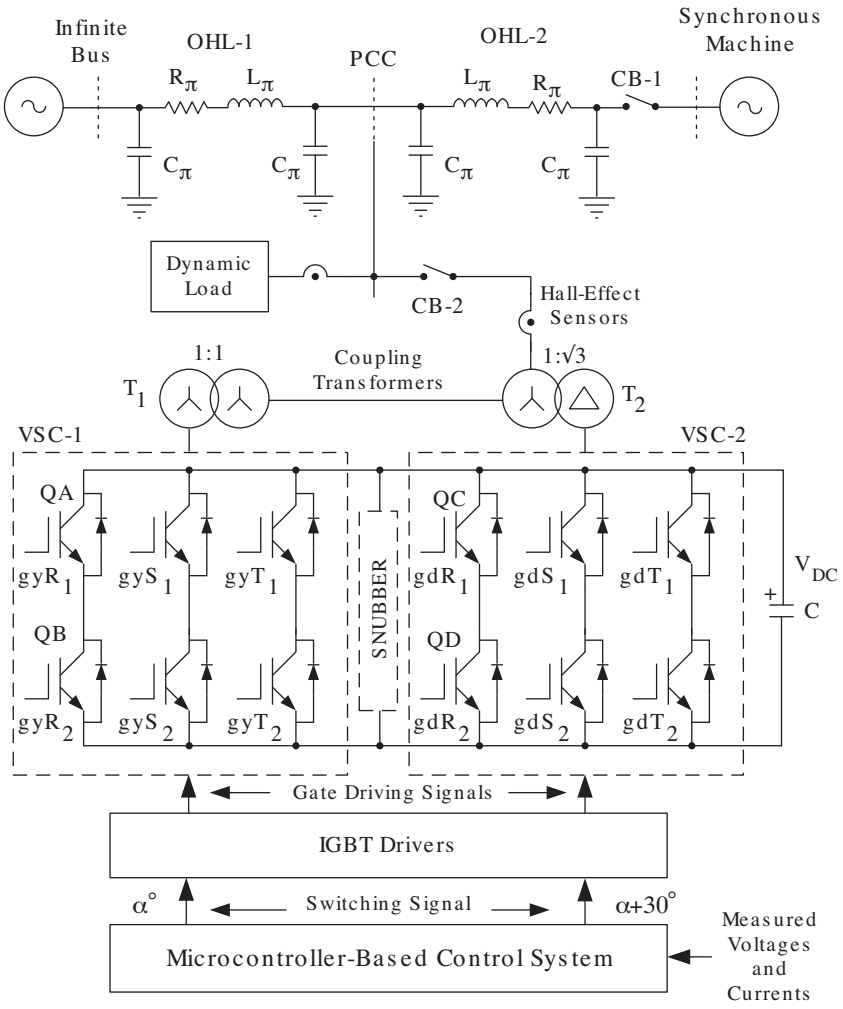


**Figure 1.** The single-line diagram of the entire system under study.

## 3. Design of the microcontroller-based control system

The STATCOM was controlled with the assistance of 3 controller cards, where each of these cards consisted of 4 microcontrollers. The clock signal, which is required for the microcontrollers, is generated by a single 10-MHz crystal oscillator on the control cards. With the use of a programmable phase-locked loop circuit inside the microcontroller, the internal clock frequency has been increased to 40 MHz and the instruction cycle has been increased to 25 ns [12]. The general block scheme of the controller card belonging to the R phase in connection with the peripheral units is displayed in Figure 2. The controller card for the R phase differs from those of the other phases only with respect to its shift register circuit. Finally, each controller card performs the duties described in the following section.

### 3.1. Generation of the control and synchronization signals

One of the most important parts of the control system is the synchronization circuit. The generation of the switching signals, computation of the active and reactive current components, serial communication among the microcontrollers, and synchronized operation are fully dependent on the synchronization signal. The synchro-

nization signal in each controller card is obtained by utilizing a zero-crossing detector and PIC1 microcontroller. The phase voltage of the AC system is applied to the zero-crossing detector from the 2 × 8 V secondary output of the supply transformer that provides power to the power supplies. The crossing of voltage wave shape from the positive cycle to the negative cycle, or vice versa, is detected with a zero-crossing detector. These 2 state signals generated by the zero-crossing detector were applied to the external interrupt inputs of the PIC1 microcontroller. Depending on the interrupt signals, the PIC1 microcontroller is used for the purpose of generating control signals ($\theta$) corresponding to 0°–180°, 30°–210°, and 90°–270° instantaneous values of the voltage wave shape, as well as the synchronization signal. The flow diagram for the PIC1 microcontroller is given in Figure 3. Any change in the system frequency will change the control and synchronization signals. These generated control signals are applied to the interrupt inputs of the other microcontrollers on the control card.

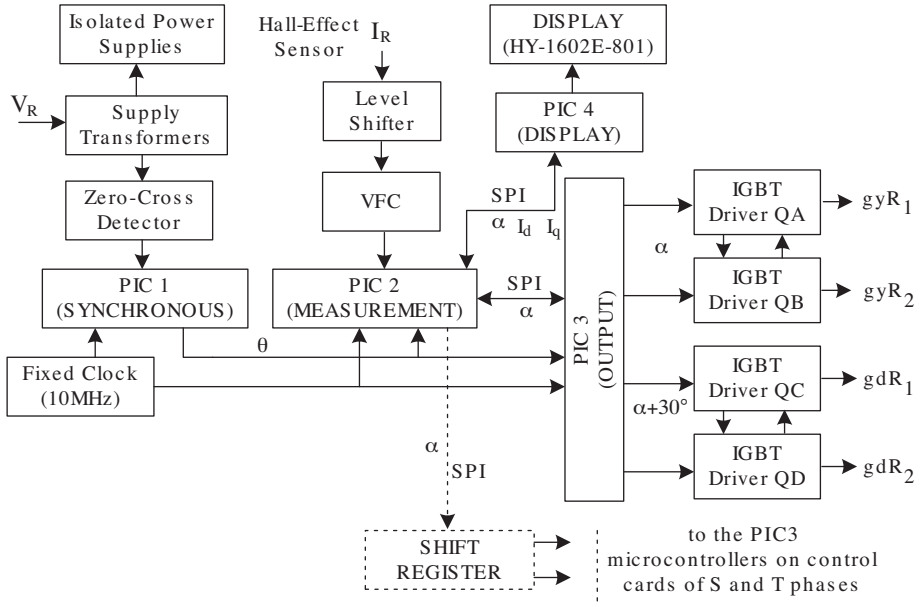


**Figure 2.** Block scheme of the microcontroller based controller card belonging to the R phase.

### 3.2. Measurement of the active and reactive current components

LA55-P/SP1 Hall-effect current sensors are used to monitor the analog currents of the 3 phases of both the STATCOM and the AC grid. The phase currents of STATCOM and AC grid are converted to an analog voltage signal by the measurement resistors connected to the output of these Hall sensors. In order to measure this analog voltage signal in both the positive and negative cycles, the offset values of the Hall-effect sensor output voltages are shifted above the time axis with the assistance of a level-shifting circuit. These analog voltage signals are converted to digital signals at the voltage-to-frequency converters. These digital signals can be used to determine the frequency and amplitude of the analog voltage signals by taking their count for a specified time interval. For that purpose, two 16-bit timers, which use the same clock input as the PIC2 microcontroller, are used to count these pulses. By selecting different starting points for the timers, both the active and reactive components of the analog input signal can be measured.

The measurement method is displayed in Figure 4 for 3 different modes of operation, namely the resistive (0° phase difference), inductive (90° phase lag), and capacitive (90° phase lead) modes. This measurement method is carried out with the assistance of PIC1 and PIC2 microcontrollers located on the controller cards.

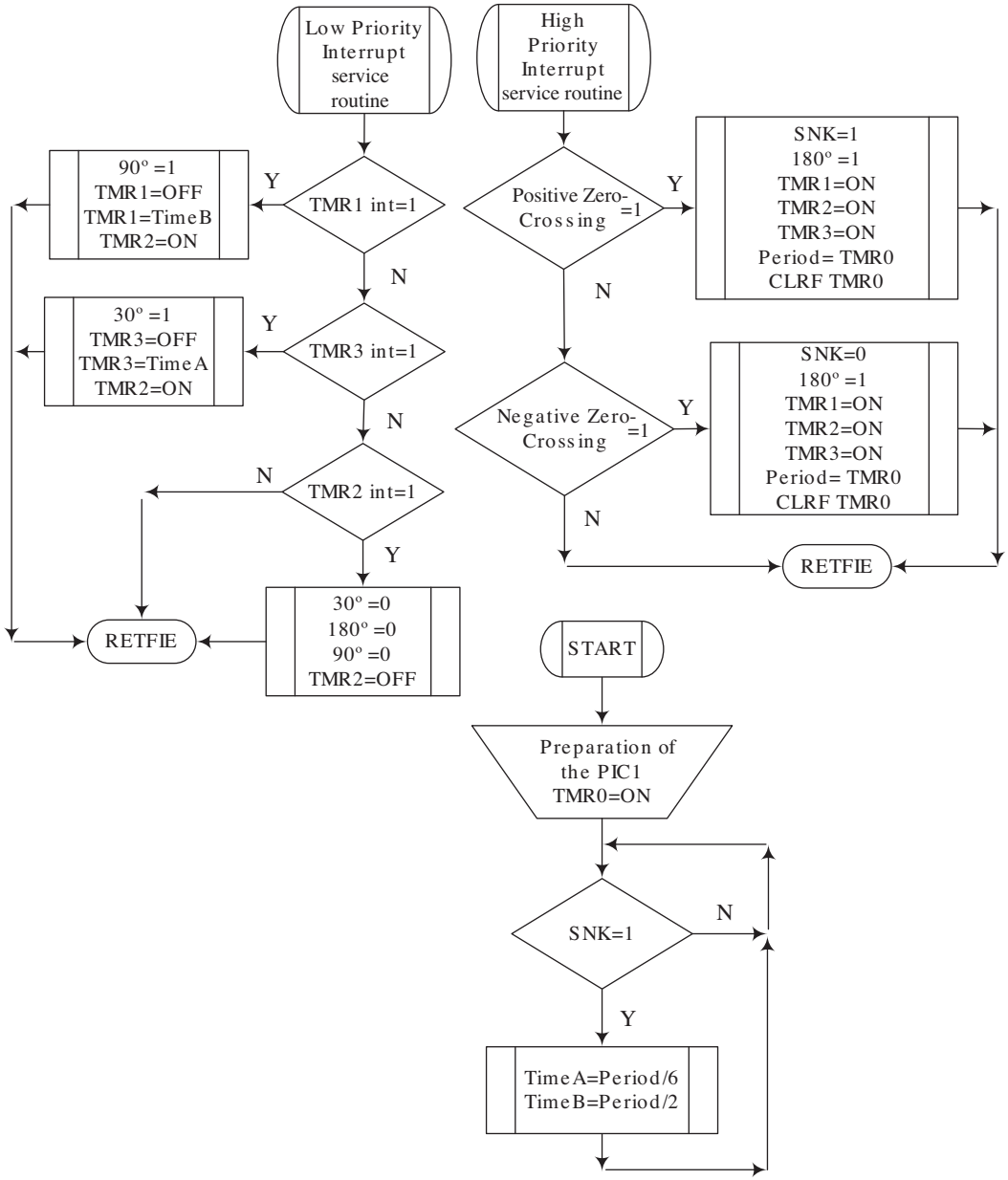


**Figure 3.** The low and high priority interrupt service routine and general flow diagram of the PIC1 microcontroller belonging to the R phase.

The flow diagram of the PIC2 microcontroller is shown in Figure 5. The PIC2 microcontroller's higher priority interrupt service routine is used for the calculation of the active current and its lower priority interrupt service routine is used for the calculation of the reactive current. The higher priority interrupt service routine is activated by control signals that belong to the positive and negative zero-crossing of the voltage (0°–180°). On the other hand, the lower priority interrupt service routine is activated by control signals that belong to the positive and negative peak values of the voltage (90°–270°). Whenever these service routines are active, the timers are reset after the number of high frequency pulses applied to the microcontroller's clock input is assigned to a specific variable. These variables, as seen in Figures 4 and 5, are named Area1 and Area2 for the active

current and Area3 and Area4 for the reactive current. Despite the fact that the areas are calculated within a single period of voltage wave shape, these areas are displayed in the same plot but at different time intervals in Figure 4 to reduce the complexity and provide coherence. The active and reactive components of the current at the completion of a full period of reference voltage are obtained by taking the difference between these variables (active current = Area1 – Area2 and reactive current = Area3 – Area4). In addition, depending on its value and sign, the calculated reactive current component is compared with a reference value in the software loop. The comparison is then used to determine the required shifting angle ($\alpha$) for the power switches. The data pertaining to this angle value are then sent via serial communication to the PIC3 microcontroller, where the switching signals are generated, as well as to the PIC4 microcontroller belonging to the displays.

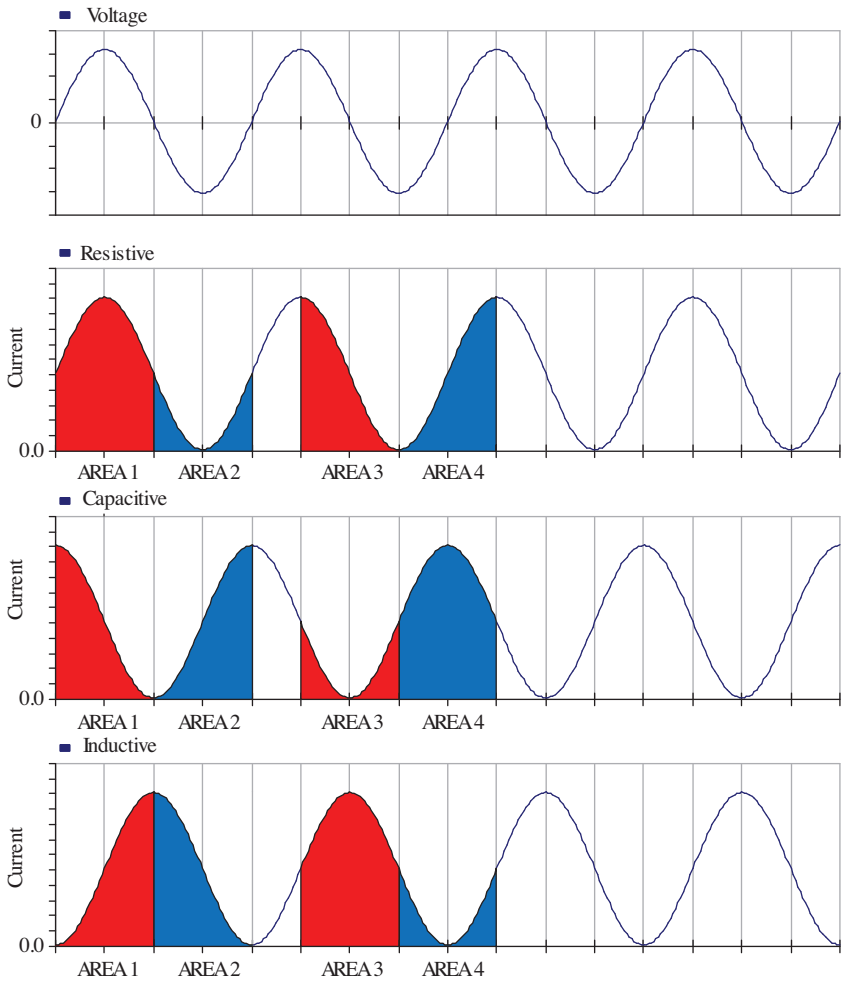


**Figure 4.** Active and reactive current reading technique.

### 3.3. Generation of the switching signals

The conventional multiple-pulse converter is based on a 3-phase bridge and only has 1 DC capacitor for the 3 phases. Thus, it is in practice difficult to control the converter currents and voltages independently on the 3 phases [9]. Therefore, the shifting angle calculated by the PIC2 microcontroller is sent to the PIC3 microcontroller and also to a shift register circuit through serial communication. The 74LS595 integrated

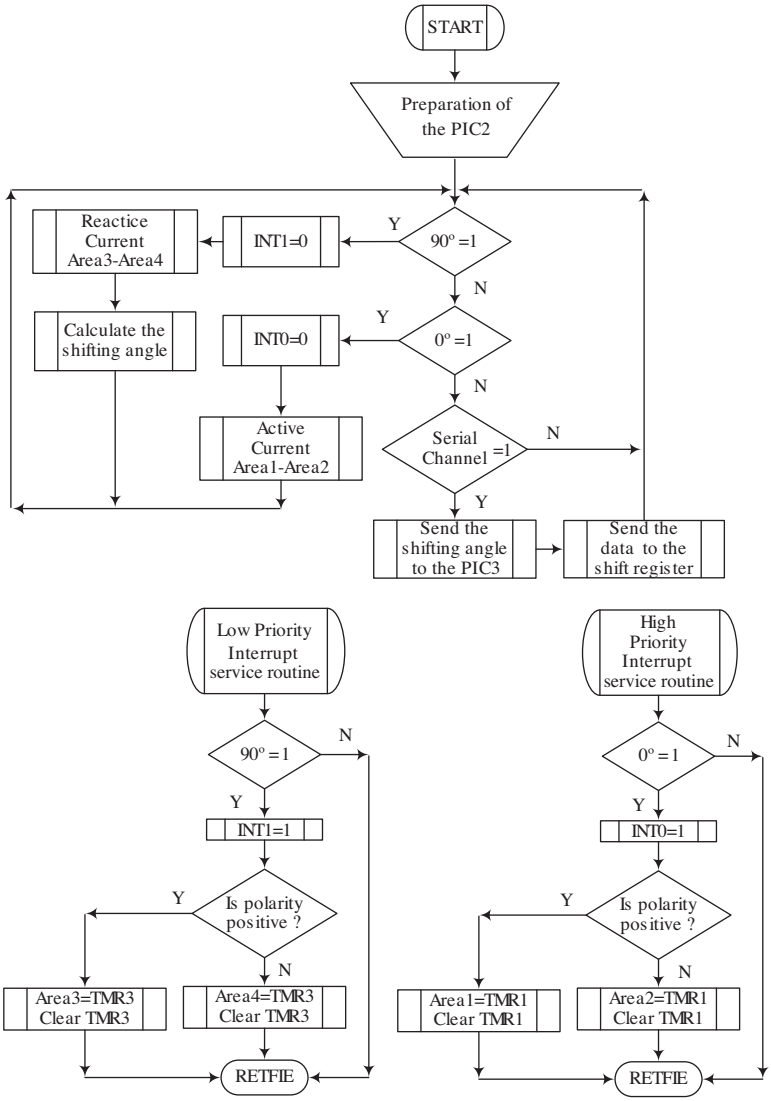


**Figure 5.** The low and high priority interrupt service routine and general flow diagram of the PIC2 microcontroller belonging to the R phase.

circuit on the shift register circuit converts the data coming through the serial data bus to a parallel data bus. The shifting angle data for the R phase on the parallel data bus are converted back to a serial by the 74LS165 integrated circuit and conveyed to the PIC3 microcontrollers on the control cards of the S and T phases.

The switching signals required by the IGBT switches in the converter bridges of the STATCOM are obtained from the PIC3 microcontrollers located on the controller cards. The flow diagram for the PIC3 microcontroller is displayed in Figure 6. As noted in Section 2, the converter bridges of the STATCOM are connected to the star and delta secondary windings of the coupling transformers. There is a 30° phase difference between the output voltages of these windings, and hence a 30° phase difference must similarly exist between the switching signals to be applied to the converter bridges connected to these windings in order to accomplish the switching of these converter bridges once per period of the AC system frequency. One of these phase-different switching signals is obtained from the control signal that belongs to the zero-crossings of the AC system voltage (0°–180°), whereas the other signal is obtained from a control signal with a 30° phase difference (30°–210°)

relative to the first signal. Whenever these control signals are active, timers that set the on-state duration of the switches on the converter bridges would be activated. The timers' set value is determined according to the angle data received from the PIC2 microcontroller. In addition, a 10-$\mu$s dead time was placed between the switching signals to prevent the upper and lower switches of each bridge from being in conduction simultaneously. In addition, the logic-level control signals generated by the PIC3 microcontrollers are not powerful enough to directly switch the IGBT's. Therefore, a IXDD 414 driver chip is used as an interface in IGBT driver cards.

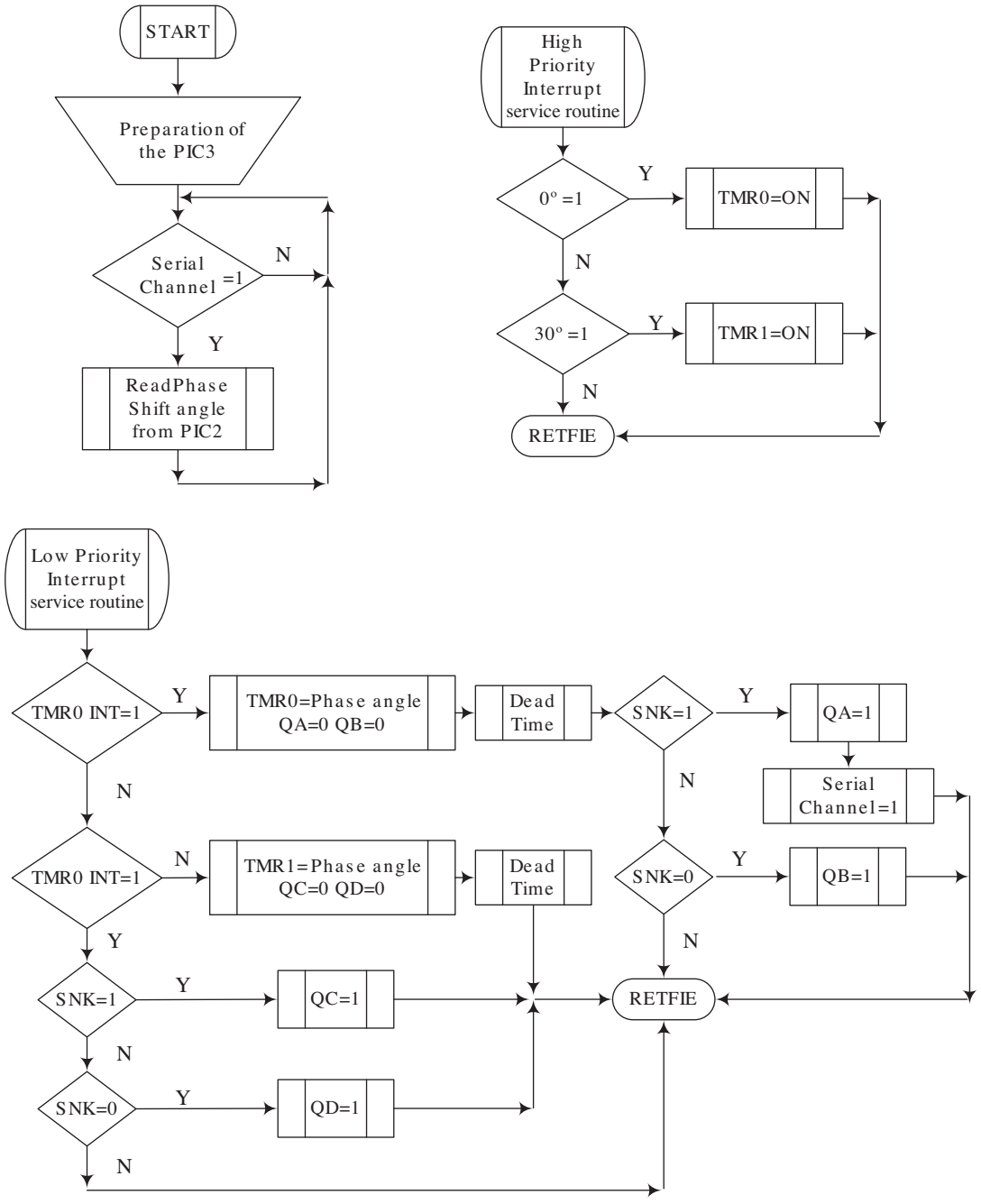


**Figure 6.** The low and high priority interrupt service routine and general flow diagram of the PIC3 microcontroller belonging to the R phase.

## 4. Experimental results

In this section, the validity of the control system has been verified by the results obtained from the experimental study. The laboratory setup established to analyze the designed STATCOM and microcontroller-based control system is shown in Figure 7. The technical characteristics of the laboratory parts are given in Tables 1–6. Measurements were taken from the experiment setup for approximately 4 min.

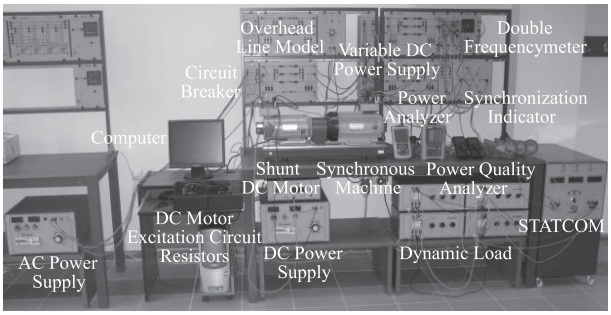


**Figure 7.** Laboratory setup used for the experiment.

**Table 1.** Power system engineering laboratory parameters used in experiment.

| | |
|---|---|
| Variable 3-phase AC power supply | 380 V (RMS), 10 A |
| Three-phase power circuit breakers | Contact load capability 400 V, 3 A |
| Inductive load controlled by 3 switches with 7 steps each | 900 VAR, 380/220 V, Y/$\Delta$ |
| Resistance load controlled by 3 switches with 7 steps each | 1200 W, 380/220 V, Y/$\Delta$ |

**Table 2.** Overhead power transmission line model parameters.

| | |
|---|---|
| Overhead power transmission line | 360 km, 380 kV, and 1000 A |
| Scale factor | 1:1000 |
| Line resistance | 13 $\Omega$ |
| Line inductance | 290 mH |
| Earth resistance | 11 $\Omega$ |
| Earth inductance | 250 mH |
| Earth capacitance | 1 $\mu$F |

**Table 3.** The 3-phase synchronous machine parameters used in the experiment.

| | |
|---|---|
| Rated appear power | 1.1 kVA |
| Rated voltage | 220/380 V $\Delta$/Y |
| Current | 2.9/1.7 A $\Delta$/Y |
| DC rotor excitation winding voltage and current | 175 V/0.47 A |
| Speed | 3000 min$^{-1}$ |

**Table 4.** DC shunt machine parameters used in the experiment.

| | |
|---|---|
| Power | 1.8 kW |
| Voltage | 220 V |
| Current | 10.5 A |
| Excitation voltage and current | 140 V/0.58 A |
| Speed | 3000 min$^{-1}$ |

**Table 5.** Parameters of the prototype STATCOM.

| | |
|---|---|
| Power device (IGBT) | IXDH30N120D1, $V_{CES}$ = 1200 V, $I_C$ = 60 A |
| DC voltage | $V_{DC(high)}$ = 500 V, $V_{DC(low)}$ = 200 V |
| DC capacitor capacitance | C = (330 $\mu$F/4) 83 $\mu$F/400 V |
| Coupling transformers (T1) | |
| Appear power | 600 VA |
| Primary winding inductance | 3 H |
| Secondary winding inductance | 3 H |
| Conversion ratio | 1:1 |
| Primary/secondary voltage | 110 V/110 V, Y/Y |
| Coupling transformers (T2) | |
| Appear power | 600 VA |
| Primary winding inductance | 3 H |
| Secondary winding inductance | 9 H |
| Conversion ratio | 1:$\sqrt{3}$ |
| Primary/secondary voltage | 110 V/190 V, Y/$\Delta$ |

**Table 6.** Measurement equipment used in the experimental study.

| Equipment | Software |
|---|---|
| Fluke 43B Power Quality Analyzer* | FlukeView Power Quality Analyzer Software, version 3.10.1 |
| HT SKYLAB 9032 Power Quality Analyzer** | Toplink Software, version 2.09 |

*Available at http://www.pqmeterstore.com/crm_uploads/fluke_43b_power_quality_analyzer_datasheet.pdf.
**Available at http://www.infotestcihazlari.com/dosyalar/pdf/gucanalizoru/HT-9032.pdf.

In the first stage, the load bus at the end of the long transmission line is supplied by the infinite bus for a duration of 55 s. As seen in Figure 8, the root mean square (RMS) values of the phase currents drawn by the load over the transmission lines for the R, S, and T phases are 725 mA, 686 mA, and 752 mA, respectively.

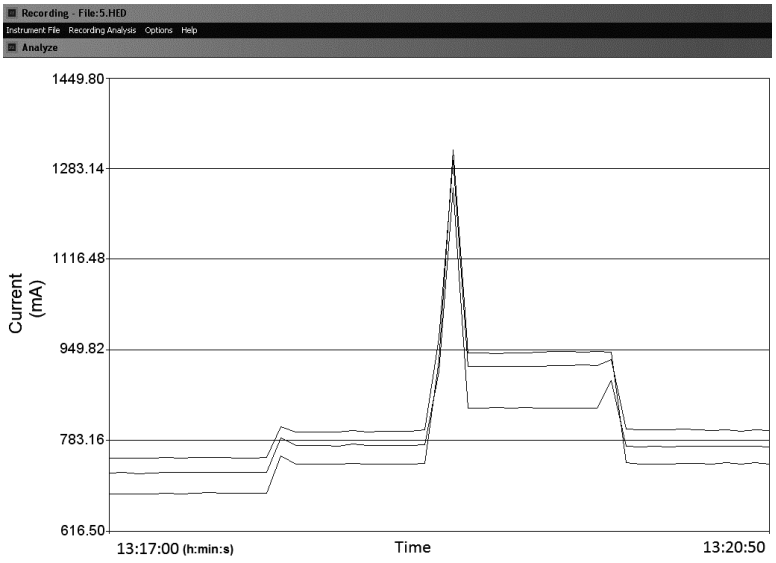


**Figure 8.** The RMS variation graph of the phase currents drawn from the PCC.

As seen in Figure 9, the active and reactive components of these currents induce a voltage drop at the serial impedance of the transmission line. Consequently, the RMS value of the phase voltages in the load bus fell back to 176 V, 185 V, and 178 V for the R, S, and T phases, respectively. The imbalance between the phase voltages arises from the infinite bus. The total power consumed at the load bus belonging to the 3 phases corresponding to these current and voltage values is 308 W, 237 VAR, and 388 VA, respectively, as shown in Figure 10. As seen in Figure 11, due to this reactive power drawn over the transmission line, a 45.5° phase difference is induced between the current and voltage waves belonging to the R phase.

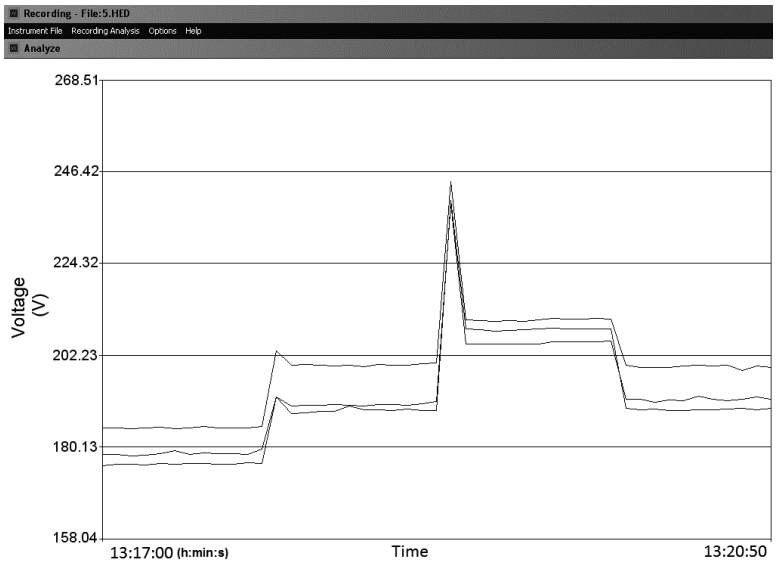


**Figure 9.** The RMS variation graph of the phase voltages belonging to the PCC.

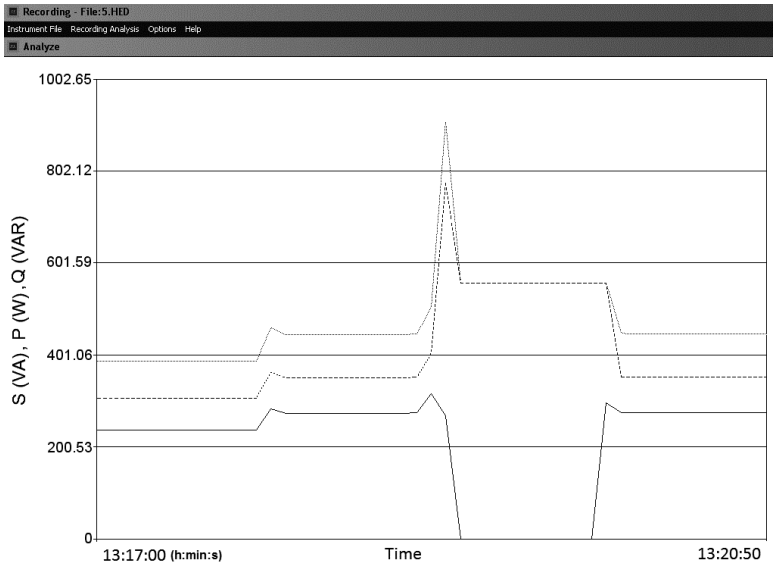


**Figure 10.** The 3-phase powers at the PCC.

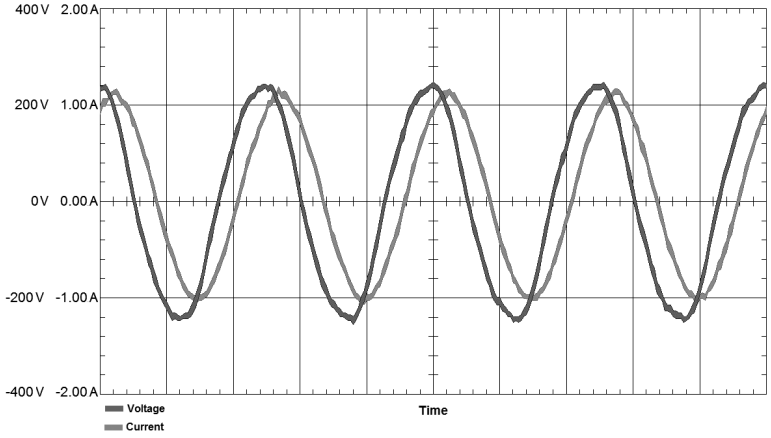


**Figure 11.** The current and voltage of the R phase at the PCC (without STATCOM and generator, time/Div = 8 $\mu$s/Div, V/Div = 200 V/Div, A/Div = 1 A/Div).

At the second stage, a symmetrical transmission system was obtained by connecting the load bus to the synchronous machine over a second transmission line with equivalent parameters to the other line. During this stage, the load is fed from both the infinite bus and bus with the synchronous machine for approximately 55 s. The current belonging to the load bus is equally drawn from both the infinite bus and the synchronous machine as a result of symmetrical feeding. Therefore, the transmission line that formerly supplied the entire load current now supplies half of this current. As a result, the voltage drop over the serial impedance of the line components decreased, as seen in Figure 9, and the RMS values of phase voltages at the load bus for the R, S, and T phases jumped to 189 V, 200 V, and 190 V, respectively. Since the initial line voltages of the symmetrical line are constant, this voltage rise obtained from the load bus caused an increase in the power and current transmitted over the line, as seen in Figures 10 and 8, respectively. The power values for the 3 phases belonging to the PCC increased to 351 W, 274 VAR, and 445 VA, while the RMS values of the phase currents for the R, S, and T phases rose to 774 mA, 740 mA, and 799 mA, respectively. It was observed that the phase difference between the current and voltage waves for the R phases did not change as a result of the symmetrical supply,

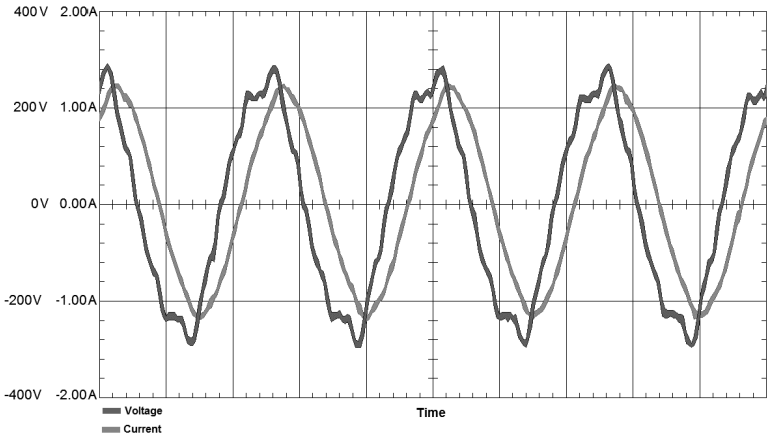


**Figure 12.** Current and voltage of the R phase at the PCC (with generator, time/Div = 8 $\mu$s/Div, V/Div = 200 V/Div, A/Div = 1 A/Div).

as shown in Figure 12. Moreover, the voltage wave shape was distorted since the synchronous machine did not produce a smooth output voltage, and thus the state of imbalance between the phase voltages was exacerbated further.

At the third stage, the parallel-connected STATCOM device was put into use and stayed operational for 60 s. As seen in Figures 8 and 9, the RMS values of the phase currents and voltages belonging to the PCC during the course of charging the DC bus capacitors temporarily increased to 1318 mA and 245 V, respectively, in conjunction with the STATCOM's engagement. Upon maintaining the compensation, the reactive power demanded by the load begins to be supplied by the STATCOM and the power transmitted over the transmission line increases. As seen in Figure 10, the total 3-phase power values belonging to the point of common coupling are 558 W, 0 VAR, and 558 VA. Due to reactive current drawn from the line segments, the voltage drop over the serial reactance of the transmission lines decreased, and the RMS values of phase voltages at the PCC for phases R, S, and T jumped to 209 V, 211 V, and 205 V, respectively, as seen in Figure 9. Likewise, the RMS values of the phase currents for the R, S, and T phases increased to 844 mA, 944 mA, and 920 mA, respectively, as displayed in Figure 8.

While the imbalances among the phase voltages are equally shared between the phases as the STATCOM is engaged, it is seen that the imbalanced phase currents are drawn from the PCC. The reason is that the imbalanced 3-phase current needed to balance the AC system's voltage is supplied by a single capacitor in the STATCOM's voltage source converter [9]. Additionally, it is seen in Figure 13 that the current and voltage wave shapes for the R phase exhibit the same phase but high levels of harmonic components. The connection type used in the STATCOM's coupling transformers could not eliminate the harmonic components under the imbalanced operating conditions. In order to reduce the harmonic components in the output voltage signals and rebalance the imbalanced supply voltage, various modulation techniques and/or filtering circuits like PWM and SHE could be employed.

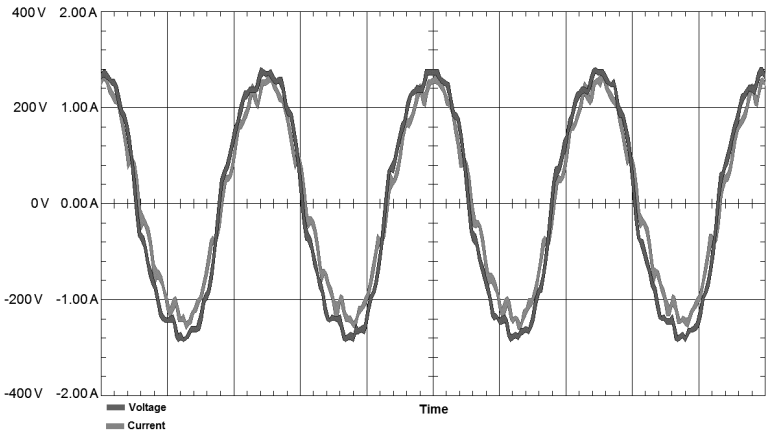


**Figure 13.** Current and voltage of the R phase at the PCC (with STATCOM, time/Div = 8 $\mu$s/Div, V/Div = 200 V/Div, A/Div = 1 A/Div).

The measurement procedure was finalized after the load bus was operated over the symmetrical supply for 60 s without the STATCOM during the fourth stage, similar to the second stage. The system reverted back to its pre-STATCOM condition upon the disengagement of the STATCOM.

### 4.1. Simulation results

The SMIB and microcontroller-based control system was simulated in PSCAD/EMTDC software. The programming codes written for the microcontroller in machine language using MPLAB software were translated to the simulation program using the C programming language. The simulation models using these programming codes were created by the PSCAD software's graphical interface. For the PSCAD synchronous machine model, the initial terminal voltage magnitude and the bus voltage angle are determined from the steady-state simulation of the power system as 1 pu and 0.251 rad, respectively.

The scenario used in the experimental study was identical to that used in the simulation study to render the results comparable. The simulation time was deliberately kept shorter than the experiment's duration in order to limit the size of the data and computation time in the simulation program. The simulation study was conducted for a duration of 5 s with time steps of 50 $\mu$s. The simulation results were obtained in such a manner that would contain the data pertaining to both transient and steady states of the system. Moreover, unlike the experimental study, the simulation studies were conducted with balanced 3-phase AC system voltages.

At the first stage, the phase currents temporarily increased while powering the line due to the finite line capacity. These phase currents have RMS values for the R, S, and T phases of 930 mA, 770 mA, and 790 mA, as seen in Figure 14. Upon reaching the steady-state operating condition, the load draws equivalent currents of 730 mA from all 3 phases as a virtue of balanced supply. The balanced phase currents drawn over the transmission line are balanced and have a potential of 177 V, as seen in Figure 15. The total 3-phase power values corresponding to these current and voltage values at the end of the transmission line are 307 W, 237 VAR, and 387 VA, as displayed in Figure 16. Moreover, temporary voltage fluctuations were observed over the line during the charging of the line capacity. In a similar way with the experimental study, a 45.5° phase difference is present between the current and voltage wave signals for the R phase exhibited in Figure 17.

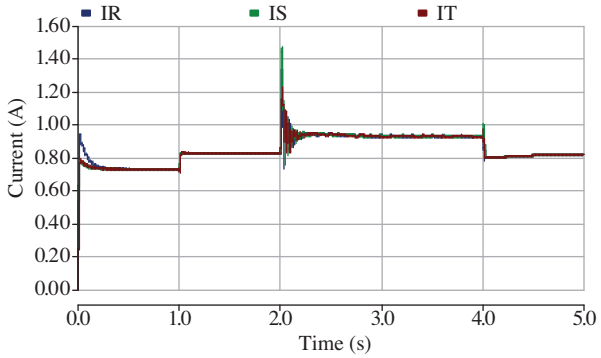


**Figure 14.** The RMS variation graph of the phase currents drawn from the PCC.

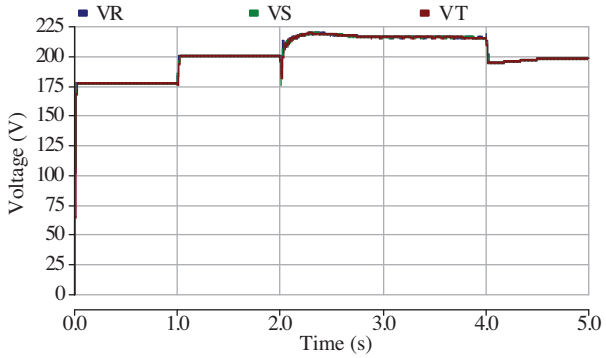


**Figure 15.** The RMS variation graph of the phase voltages belonging to the PCC.

During the second stage, the RMS values of the phase currents and voltages drawn from the point of common coupling increased to 823 mA and 199 V due to the symmetrical and balanced feeding, as seen in Figures 14 and 15. Thus, the total 3-phase power values measured from the common coupling point rose to 391 W, 301 VAR, and 491 VA, as seen in Figure 16. As a virtue of balanced feeding, no visible distortion occurred in the current and voltage wave shapes belonging to the R phase shown in Figure 18. Likewise, the phase difference between these wave signals did not change, either.

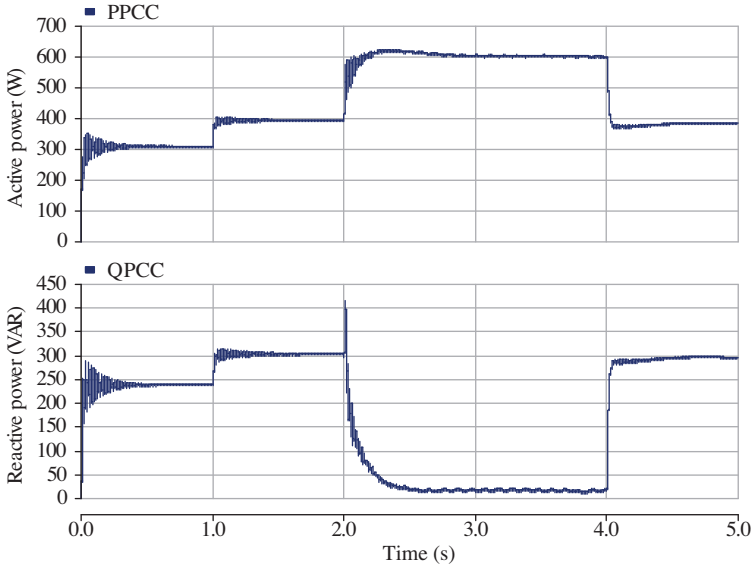


**Figure 16.** 3-Phase powers at the PCC.

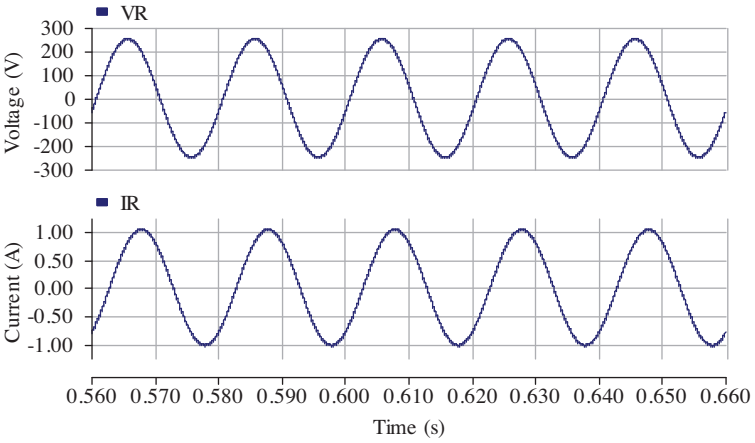


**Figure 17.** Current and voltage of the R phase at the PCC (without STATCOM and generator).

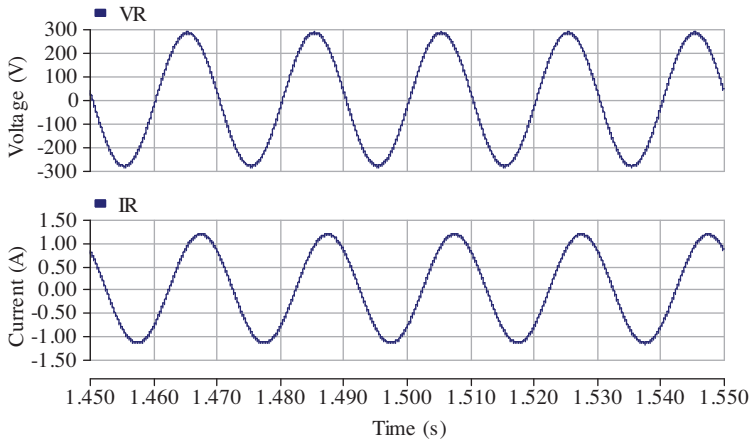


**Figure 18.** Current and voltage of the R phase at the PCC (with generator).

Similar to the experimental study, the RMS value of the phase currents during the charging of the STATCOM's DC bus capacitor temporarily rose to as high as 1450 mA in the third stage, as seen in Figure 14. Within the steady state conditions, the RMS value of these phase currents is on the level of 928 mA. As shown in Figure 15, the phase voltages were balanced and escalated to 215 V, differing from the experimental study. The total 3-phase power values are 600 W, 11 VAR, and 597 VA, as seen in Figure 16. As a virtue of the balanced supply, the current and voltage wave signals belonging to the R phase as shown in Figure 19 contain only the high level harmonics induced by the 12-pulse operation, as the low-level harmonics were eliminated by the coupling transformers. Finally, a negligible phase difference persisted between the voltage and current wave signals for the R phase as the reactive power value could not be completely zeroed.

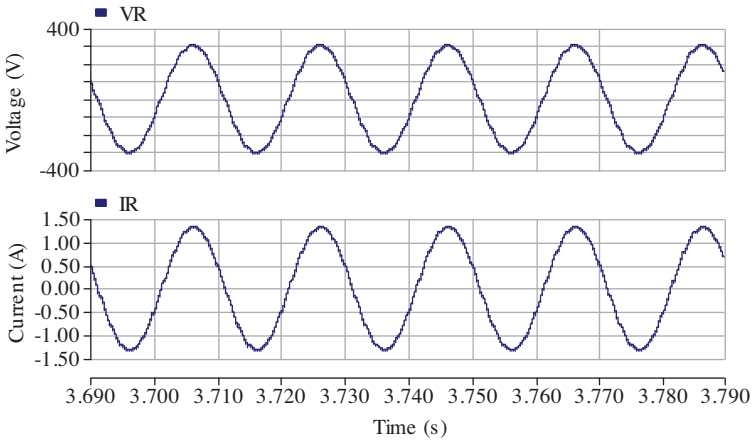


**Figure 19.** Current and voltage of the R phase at the PCC (with STATCOM).

## 5. Conclusion

In this study, design of a microcontroller-based control system was presented for a laboratory-size prototype of a STATCOM with the structure of a VSC, which was able to regulate the voltage and provide reactive power compensation in order to improve the performance of the AC transmission system. The control system was implemented with low-cost 16-bit microcontrollers. In order to obtain reactive power compensation with a unity power factor, the nonactive power theory was applied to the microcontroller-based control system. The suitability of the developed methodology for the determination of the reference reactive current components, for resistive and inductive operating conditions, was demonstrated with plots. The calculation of the reference reactive current components was performed without resorting to complex mathematical manipulations that would delay the compensation process.

Experimental and simulation studies were conducted on a SMIB power transmission system in order to verify the validity of the control system. Specifically, disturbances in the AC system voltage caused by the connected synchronous machine to the grid did not interfere with the operation of the controller. For this reason, it can be proposed that the designed control system is suitable for the compensation of balanced and/or imbalanced single-phase or 3-phase systems with sinusoidal and/or nonsinusoidal periodical voltage wave shapes. Nevertheless, harmonics observed at the output voltage and/or the current wave shape of the STATCOM could not be removed due to imbalanced working conditions as well as the multipulse STATCOM architecture.

**Acknowledgment**

This work was supported in part by the Scientific and Technological Research Council of Turkey (TÜBİTAK) under project number 104M235.

## References

[1] B. Singh, R. Saha, A. Chandra, K. Al-Haddad, "Static synchronous compensators (STATCOM): a review", IET Power Electronics, Vol. 2, pp. 297–324, 2009.

[2] L. Gyugyi, "Application characteristics of converter-based FACTS controllers", International Conference on Power System Technology, Vol. 1, pp. 391–396, 2000.

[3] L.M. Tolbert, T.G. Habetler, "Comparison of time-based non-active power definitions for active filtering", 7th IEEE International Power Electronics Congress, pp. 73–79, 2000.

[4] A. Bhattacharya, C. Chakraborty, S. Bhattacharya, "Shunt compensation", IEEE Industrial Electronics Magazine, Vol. 3, pp. 38–49, 2009.

[5] H. Okyere, M. Nibouche, H. Nouri, O. Al Mrayat, "Application of DSPS and microcontrollers in voltage source inverters STATCOM digital designs: a comparative approach", IEEE International Conference on Signal Processing and Communications, pp. 321–324, 2007.

[6] C. Qian, M.L. Crow, S. Atcitty, "A multi-processor control system architecture for a cascaded StatCom with energy storage", 19th Annual IEEE Applied Power Electronics Conference and Exposition, pp. 1757–1763, 2004.

[7] L. Xu, V.G. Agelidis, E. Acha, "Development considerations of DSP-controlled PWM VSC-based STATCOM", IEE Proceedings in Electric Power Applications, Vol. 148, pp. 449–455, 2001.

[8] Y. Xu, L.M. Tolbert, F.Z. Peng, J.N. Chiasson, J. Chen, "Compensation-based non-active power definition", IEEE Power Electronics Letters, Vol. 1, pp. 45–50, 2003.

[9] K.K. Sen, "STATCOM-STATic synchronous COMpensator: theory, modeling, and applications", IEEE Power Engineering Society 1999 Winter Meeting, Vol. 2, pp. 1177–1183, 1999.

[10] Y. Xu, L.M. Tolbert, J.D. Kueck, D.T. Rizy, "Voltage and current unbalance compensation using a static var compensator", IET Power Electronics, Vol. 3, pp. 977–988, 2010.

[11] Y. Xu, L.M. Tolbert, J.N. Chiasson, J.B. Campbell, F.Z.Z. Peng, "A generalised instantaneous non-active power theory for STATCOM", IET Electric Power Applications, Vol. 1, pp. 853–861, 2007.

[12] MicroChip Technology Inc., PIC18FXX2 Data Sheet, pp. 17–20. Available at: http://www.micro.deis.unibo.it/∼campi/ESD_2004/manuali/pic18fxx2.pdf.